Enhancing the stability of ω phase in zirconium alloys via local interlayer twists

Enhancing the stability of ω phase in zirconium alloys via local interlayer twists

Hongjiang Li [1], Long Zhao [1], Hongxiang Zong [1,*], Xiangdong Ding [1,*], Turab Lookman[1], Jun Sun [1], Graeme J. Ackland [2]

[1]*State Key Laboratory for Mechanical Behavior of Materials, Xi'an Jiaotong University, Xi'an, Shaanxi 710049, China*

[2]*Centre for Science at Extreme Conditions and School of Physics and Astronomy, The University of Edinburgh, Edinburgh, EH9 3FD, United Kingdom*

*To whom correspondence should be addressed.

E-mail: zonghust@mail.xjtu.edu.cn, dingxd@mail.xjtu.edu.cn

Abstract

The addition of solute provides an effective means to alter the stability of phases in metallic materials. This is particularly true for the metastable ω phase in Ti- and Zr-based alloys, however, the underlying mechanism remains inconclusive. In the present work, we show that the ω→β phase transformation process can be hindered to stabilize the ω phase over a wide temperature and pressure range. This is demonstrated by molecular dynamics (MD) simulations of Zr-Nb alloys. In particular, we show that Nb dopants lead to the formation of a novel defect structure in the Zr-ω phase, i.e., there is a co-rotation of 6 atoms in the {0002} plane by 30° along the c-axis of the ω lattice. We refer to this as a local interlayer twist (LIT). The LITs are energetically preferred within Nb-rich regions and can interlock ω lattices, thus retarding the ω→β phase transformation. Furthermore, our DFT calculations suggest that this mechanism should work in Zr- and Ti-based alloys with small solute atoms. The findings enrich our understanding of complex phase transformation kinetics in alloys.

I. INTRODUCTION

Structural phase transformation controls the behavior of materials systems such as shape memory alloys, steels and functional ceramics. Their properties can be tailored by changing the phase stability and phase transformation behavior [1-3]. This is often achieved by doping with defects or alloying elements [4,5]. Thermodynamically, element doping can influence the relative stability of specific phases or induce metastable phases [6]. For example, doping β-stabilizing elements (such as Nb, V, Mo, etc.) can endow Ti- and Zr-based alloys with a greater volume fraction of the β phase, i.e., decrease the free energy of the β phase relative to other phases [7-10]. More importantly, alloying elements can change the kinetics of the phase transformation, crucial to determining phase stability. On the one hand, dopants can influence the nucleation barrier of the product phase, which governs the incubation time and starting transition temperatures or pressures of the new phase [11,12]. On the other, solute atoms can induce local lattice distortion or change the local chemical environment, thus altering the growth process in new phases [13-16].

The metastable ω phase that can be formed in β-Ti or β-Zr alloys serves as an ideal testbed for understanding the alloying effect on phase stability. The ω phase is a hexagonal structure (space group P6/mmm) with three atoms per unit cell. The geometry is very layered: the first layer (A) is filled by atoms at the Wyckoff position (0, 0, 0), and the next layer (B) consists of atoms at the Wyckoff positions (2/3, 1/3, 1/2) and (1/3, 2/3, 1/2) [17]. In Ti- or Zr-based alloys, either rapid quenching [18,19] or isothermal aging [20] can induce the ω-phase, for which the transformation mechanism can be well described by the collapse of the $\{111\}_\beta$ plane [17]. However, the effect of alloying makes the phase transformation behavior more complex. In addition to changing the free energy difference between the β and ω phases [21,22], alloying can also give rise to incomplete $\{111\}_\beta$ collapse [23-25], a change in the "collapse-diffusion" transformation pathway [26], and local lattice mismatch that can influence β↔ω transformation kinetics [27,28]. In these scenarios, the stability of the ω phase is influenced by either changing the transformation pathway or introducing an elastic field.

Less is known about other mechanisms that can stabilize the ω phase in Ti- or Zr-based alloys.

In the present work, we report a mechanism that can retard the ω→β phase transformation and stabilize the ω phase in Zr-based alloys. With the help of a machine learned potential and molecular dynamics (MD) simulations, we show a novel defect structure in the ω phase in which two neighboring A-B layers are twisted relative to each other by 30° locally (hereafter referred to as the local interlayer twist, LIT). In the following, we demonstrate that these unique LIT defects can interlock the ω lattice at high temperatures, thus stabilizing the ω phase over a wider temperature region at different pressures. More importantly, the finding suggests that the phase transformation kinetics cannot be ignored in describing the phase diagram and mechanical behavior of Ti- or Zr-based alloys at high pressure. The paper is organized as follows: In section II, we describe the the simulation details. In section III, we present the main result of this work, including the conditions for the existence of LITs as well as how they are correlated with the stability of the ω phase. In section IV, we discuss the thermodynamic and kinetic factors that are responsible for the stability of the ω phase at high temperature and we conclude in section V.

II. COMPUTATIONAL DETAILS

We employ first-principle calculations and MD simulations to capture the effect of alloying elements on the stability of the ω phase in Zr-based alloys. Here, we take the Zr-Nb alloy as an example for the MD simulations of the ω→β phase transformation. Typical Zr-Nb samples were created by randomly replacing a given atomic concentration x% (x=7.5, 10, 12.5) of Zr sites with Nb atoms. All MD simulations were initiated with a 10×8×5 supercell of ω lattices (that is, 1200 atoms). The NPT ensemble was used to control temperature and pressure, with a time step of 1 fs.

Using Zr-Nb alloy as an example, we perform the MD simulations using the Large-scale atomic/molecular massively parallel simulator (LAMMPS)[29] to capture the ω →β phase transformation. The interatomic interactions in the Zr-Nb alloy are learned

by a machine learning (ML) potential from first-principles calculations data. The ML potential was trained with kernel ridge regression (KRR) [30], which captures the nonlinear relationship between the local atomic environment and the corresponding potential energy or atomic forces. In the present study, the description of the local atomic environment is given by 132 features physically informed from the nature of the ω→β phase transformation in Ti- and Zr-based alloys. A large set of configurations were sampled using first-principle molecular dynamic simulations under different temperatures and pressures. The properties of Zr-Nb alloys, such as lattice constant, elastic constant and E-V curve agree well with DFT calculations. The details of the ML potential as well as the fitting process and properties can be found in the supplementary materials [31]. The complete details of the machine learning model and the code for LAMMPS implementation have been uploaded to https://github.com/Lihongjiang-material/Zr-Nb_ML_potential.

The first-principles calculations to check the stability of LIT in alloys made use of the Vienna ab initio simulation package (VASP) with projector augmented wave (PAW) [35]. Different types of parameters were used for the exchange-correlation function [34,39-41]. The ω phase with 288 atoms (supercell 8×4×3) was used for all first principle calculations. The LIT formation energy was estimated by calculating the changes of potential energy in Zr-10X (at. %) and Ti-10X alloys (X = Y, Cs, Hf, Cd, *et. al.*) due to adding an LIT.

III. RESULTS

Fig. 1(a) shows a typical atomic configuration for a Zr-10Nb (at. %) single crystal with the ω phase at 150 K and 0 GPa after 1 ns annealing viewed along the c-axis. The left panel shows the structure and the right panel shows the corresponding elemental distribution. Most of the ω phase survives with atoms located in their ω lattice sites, suggesting that the ω phase is stable. However, we can still observe several “interstitial” atoms (yellow atoms in Fig. 1(a) left panel) that deviate from their perfect lattice positions. These “interstitial” atoms are arranged in a manner similar to crowdion

defects [42]. However, crowdion interstitials are often observed at high temperatures or under radiation damage [43]. A closer look at the structure of the ω phase in the Zr-10Nb system indicates that these "interstitial" atoms locally form twisted inter-layers of {0002} planes. As shown in Fig. 1(b), the local inter-layer twist is the result of the co-rotation of 6 atoms within the honeycomb layer (i.e., {0002} of ω lattice) by 30° along the c-axis, akin to the structure of magic-angle graphene [44]. This unique local defect structure is quite distinct from any existing defects in close-packed metallic crystals. Hereafter, we refer to this defect structure as an "local inter-layer twist" (LIT). To rule out any artificial effect due to the interaction potential, we double checked the stability of LITs by ab initio MD simulations with different pseudopotentials (PAW-PBE-GGA, PAW-LDA, GGA91 and USPP-LDA). For each case, a ω super-lattice containing a LIT was annealed at 150 K for 6000 steps (6 ps). The initial cell of AIMD was modeled with classical MD annealing at 150 K and 0 GPa. The corresponding snapshots after annealing are shown in Fig. 1(c). The LIT structure is quite stable at finite temperatures, as demonstrated by the surviving LIT in the AIMD simulations of the ω phase.

We next investigated the stability of LITs as a function of temperature and pressure. Fig. 2(a) shows the temperature–pressure phase diagram of Zr-10Nb, in which circle symbols represent the specific temperature and pressure at which LITs survive after long-term relaxation (~1 ns), and the phase boundary is determined by the refined phase diagrams in Fig. S4. The LITs remain stable below 4 GPa, and the LIT stable temperature region decreases as a function of pressure, i.e., LITs can survive in the temperature region 100-400 K below 2GPa but only 275-325K at 4GPa. However, no LITs are activated below 100 K over the time scale of the MD simulation. Above 400 K, all ω phases transform into the β phase. This suggests that LITs act as an intermediate state between the low-temperature ω phase and high-temperature β phase. External pressure is another thermodynamic parameter that can influence the stability of LITs, i.e., the temperature region is suppressed at higher pressure. More importantly, we also analyze LITs in Zr-Nb alloys with different Nb concentrations, as shown in Figs. 2(b)

and 2(c). In Fig. 2(b), we show the LIT stability regions spanning pressure and Nb concentration. All the Zr-Nb samples are annealed at 200 K, which is a favorable temperature for LITs. We find that the maximum pressure for activating LITs decreases with the Nb concentration, consistent with the trend of the ω-β phase boundary. The same is true for the temperature threshold as a function of Nb concentration at 0 GPa (see Fig. 2(c)). Noticeably, the upper limit of the temperature threshold is more sensitive to Nb composition compared to the lower limit. It appears that the LITs are more likely to be activated in the unstable ω phase. To confirm this, we counted the number of Nb atoms within LITs in all modes. All LITs contain at least 1 Nb atom, and nearly half of the LITs have more than 2 Nb atoms (Fig. 2(d)).

Our simulations also reveal the influence of LITs on the behavior of the ω↔β phase transformation. We simulated the phase transformation in Zr-10Nb starting from a ω single crystal with and without LITs. The stability of LITs in the LIT case is manipulated by changing the average number of Nb atoms within the LIT structure, here we randomly replaced Zr atoms with Nb atoms within LITs. and the chemical arrangement of its counterpart without LITs is also updated. Fig. 3 shows the ω↔β phase transformation temperatures upon heating and cooling at 6 GPa. Under such pressure, new LITs would not be generated (Fig. 2(a)), and existing LITs would not disappear on the time scale of the simulation. Each case was repeated 5 times to ensure the reliability of our simulation results and the corresponding transformation temperatures were also averaged. As shown in Fig. 3, both the phase transformation temperatures upon heating and cooling increase with local Nb composition. More strikingly, for a specific local Nb composition, Zr-10Nb samples with LITs show both higher ω→β transformation temperatures and larger thermal hysteresis. However, the phase transformation temperatures upon cooling show little difference as all the LITs disappear when the systems transform to the β phase. The LITs can stabilize the ω phase at higher temperatures, 70 K higher than those without LITs. More importantly, this effect is enhanced as we increase the number of Nb atoms within LIT structures, i.e., the ω→β transformation temperature is increased from 420 K to 540 K after replacing another 4

Zr atoms within the LIT with Nb atoms.

IV. DISCUSSION

From a thermodynamic perspective, the stability of the ω phase can be examined by its free energy landscape. We compared the potential energy of the ω phase with and without LIT in Zr-10Nb alloys. An LIT with a selected number of Nb atoms was engineered into an ω supercell of 288 atoms. The chemical arrangement without the LIT is the same and the corresponding potential energy per atom for the ω lattice with and without an LIT is compared in Fig. 4(a). The potential energy of the system decreases slowly with higher local Nb composition without the LIT. Increasing the number of neighboring Nb atoms within {0002} layers increases the ω phase stablity, as the potential energy decreases from -8.5885 to -8.5895 eV/atom (red line in Fig. 4a). In contrast, the introduction of LIT decreases the energy to suggest that the LIT is a stable defect in the ω phase in Zr-based alloys. The potential energy of the ω phase with LITs is more sensitive to the number of Nb atoms in the LIT. As shown by the black line in Fig. 4(a), 6 Nb atoms within LIT decrease the energy of the ω supercell from -8.5895 to -8.5945 eV/atom, five times larger than that of a perfect ω lattice. In this sense, the presence of LITs with a larger number of Nb atoms stabilizes the ω phase.

We note that this is quite different from the case of a 12-atom supercell (the upper panel of Fig. 4(b)), which is the primitive unit cell of a LIT. For such a primitive unit cell, its potential energy is higher than that of the corresponding supercell without the {0002} plane rotation (the lower panel of Fig. 4(b)). This indicates that the decrease in potential energy for large supercells is due to the interaction between LITs and neighboring ω lattices. The volume change of the ω phase due to the LIT is higher by 6%. The increase in volume can decrease the elastic energy because of the size mismatch between Zr and Nb atoms.

We investigate the interaction between LITs by monitoring the potential energy change of the Zr-Nb system as function of the distance between LITs by building a supercell with size 11×11×11 of perfect ω unit cells, two of which are replaced by LIT

unit cells. The potential energy as a function of the LIT-LIT distance along three different directions (i.e., $[11\text{-}20]_\omega$ a axis, $[\text{-}1100]_\omega$ b axis, and $[0001]_\omega$ c axis) is monitored 50 times and the results averaged. As shown in Fig. 4(c), the potential energy of the supercell decreases with LIT-LIT distance for all three directions. The c axis direction shows the sharpest potential energy decay (blue curve in Fig. 4(c)), suggesting a strong repulsive interaction between LITs. In addition, the repulsive interaction becomes very weak if the LIT-LIT distance is larger than 1.5nm along a and b axes, but only 1nm for the c axis.

We consider the mechanism underlying the ω→β phase transformation in Zr-10Nb alloys in Fig. 5. Figs. 5(a) and 5(c) illustrate the transformation mechanism according to the model of $\{111\}_\beta$ collapse. It is generally believed that there are two main steps involved in the phase transformation from β to ω, i.e., every second and third {111} planes of the β phase shift toward each other (collapse) by $\frac{1}{12}\{111\}a_0$ (a_0 is the lattice parameter of the β phase), and then the atoms redistribute in the collapsed lattice through shuffling [17]. Thus, its reverse transformation process (ω→β) should be described well by the separation of the $\{111\}_\beta$ planes. As shown in Fig. 5(c), the two atoms within the $\{0002\}_\omega$ plane (red particles) move in the opposite direction along the c-axis, leading to the formation of the second and third $\{111\}_\beta$ planes. However, the transformation pathway should be modified after the formation of LITs. As illustrated in Figs. 5(b) and 5(d), the atoms within the $\{0002\}_\omega$ planes rearrange to form LIT structures. These atoms are confined to the interstitial sites of the ω lattice (yellow particles in Fig. 5), leading to a lack of atoms that can directly separate into $\{111\}_\beta$ planes. In this scenario, more complex transformation pathways should be adopted to form a perfect bcc lattice involving an additional energy barrier. This is supported by atomic configurations extracted from the high-temperature relaxation of the ω phase with LITs. Fig. 5(e) shows a typical microstructure of Zr-10Nb alloys heated to 500 K. We find that most ω lattices transform into bcc lattices (blue atoms), but a small proportion of ω lattices survive around the LIT (orange and yellow atoms). Interestingly, the surviving ω lattices are along the $[0001]_\omega$ direction, suggesting a stronger interaction

between LITs and ω lattices along the c-axis. It has been suggested that the ω→β structural phase transformation occurs in a collective manner in response to a softening of the $[0002]_{\omega}$ longitudinal phonon mode (parallel to $[111]_{\beta}$) [45]. For the ω→β transformation, the presence of LITs can scatter the propagation of the $[0002]_{\omega}$ phonon mode, thus inter-locking ω lattices nearby.

The energy barriers of the ω→β phase transformation for Zr-10Nb alloys are calculated to investigate the kinetic effect of LITs. An ω superlattice containing an LIT was utilized to explore the transition state along the ω→β phase transformation pathway with the help of the nudge elastic band (NEB) method [46,47]. We considered two of the most promising pathways, i.e., the nonbasal plane shuffle (pathway I), and the separation of the $\{0002\}_{\omega}$ planes preceding the process of LIT detwisting (pathway II). In the nonbasal plane shuffle process, the atoms within LIT directly move to the β lattice sites without separation of the $\{0002\}_{\omega}$ planes. The detwisting process is actually the reverse process in Fig. 1(b). Thus, this is a comparison between a one-step phase transformation and a two-step phase transformation. For each case, a supercell of 288 atoms was used, and there are two Nb atoms within a LIT. As shown in Fig. 6(a), the two transformation pathways have quite different energy barriers. The energy barriers of pathway I and pathway II are ~558.3 meV/atom and ~30.1 meV/atom, respectively. This indicates that pathway II is much more energetically preferred. In addition, we note that the energy barrier for LIT detwisting is higher than that for the $\{0002\}_{\omega}$ separation. In this sense, the annihilation of LITs is the prerequisite for *ω* phase destabilization. Subsequently, we investigated the influence of Nb composition within an LIT on the energy barriers associated with LIT detwisting. As shown in Fig. 6(b), we compared the energy barriers in the presence of 2 Nb, 4 Nb and 6 Nb atoms in the LIT. The energy barrier for detwisting increases with the number of Nb atoms within an LIT, i.e., the ω→β transformation barrier increased 5 fold for 6Nb in an LIT. This indicates that the kinetic stability of the ω phase strongly depends on the Nb composition within the LITs. This is responsible for the increased ω→β transformation temperature with higher Nb composition within LITs in Fig. 3.

Finally, we investigated the possibility of LITs forming in other Zr- and Ti-based alloys. The thermodynamic stability of LITs in the ω phase for Zr-X and Ti-X binary alloys is revealed using first-principle calculations [35,36]. For each case, a single crystal of the ω phase (288 atoms) with around 10% solution atoms (29 solute atoms, 10.07%) was used to calculate the LIT formation energy, i.e., the energy difference due to the formation of a LIT, $(E_{\text{with-LIT}}\text{-}E_{\text{without-LIT}})/n_{\text{atoms}}$. More negative formation energy refers to more thermodynamically stable LIT. As shown in Fig. 7(a) [48], a large proportion of Zr-based alloys possess negative LIT formation energy, suggesting LITs can be probed in most Zr alloys. More importantly, the LIT formation energy is correlated with the size difference between Zr and X atoms, i.e., r_{Zr}-r_X. LITs are only stable in these Zr alloys with smaller solute atoms favored (i.e., r_{Zr}-r_X> 0.05 Å). Presumably, relatively small solute atoms are energetically preferred to occupy interstitial positions between the host atoms. This argument is supported by the phase diagram of Ti-X alloys spanned by the LIT formation energy and the size difference between Ti and X atoms (Fig. 7(b)). For Ti-X alloys, r_{Ti}-r_X> 0.2 Å is a prerequisite for the presence of LITs.

It is important to point out that the occurrence of local segregation of solute atoms or chemical composition fluctuation is inevitable in Zr- and Ti-based alloys. This is especially true for the Zr-Nb system due to the presence of spinodal decomposition upon annealing [49]. Therefore, LITs should be a type of intrinsic defects in Zr- and Ti-based alloys at elevated temperature. In this scenario, LITs will suppress the ω→β phase transformation and increase the critical transformation temperature. As shown in Fig. 8, even doping with β-stabilizing elements (i.e., lowering the free energy of β phase relative to ω phase), the LITs can still enhance the stability of the ω phase by increasing the ω→β phase transformation barrier. This kinetic factor cannot be ignored in the understanding of mechanical performance related to ω-phase in Zr- and Ti-based alloys.

V. CONCLUSION

We examined the stability of the ω phase in unaged Zr-Nb alloys under different

pressures. The MLP trained from ab initio data has allowed us to directly simulate the thermally induced ω→β phase transformation process. We find that the higher local composition of solution Nb atoms greatly increases the stability of the ω phase in Zr-Nb alloys. At a relatively high temperature, Nb atoms can trigger a novel defect structure in the ω phase, that is, the co-rotation of 6 atoms on the {0002} plane by 30° along the c-axis of ω lattices, denoted as the local interlayer twist (LIT). The LITs increase the volume of ω lattices and release local elastic energy due to the size mismatch between the atomic species, thus decreasing the free energy of the ω phase. The thermodynamic stability of the LITs and ω phase strongly depend on the composition of Nb's within LITs. More importantly, the LITs can inter-lock the ω lattices nearby and increase the energy barrier of the ω→β phase transformation. It is suggested that this new mechanism should work in Zr-based and Ti-based alloys with relatively small solute atoms, in general.

The present findings potentially help to understand several experimental observations related to the ω-phase. It is known that the β to ω phase transformation in Zr-Nb alloys exhibits a pronounced pre-transition effect, i.e., incommensurate ω structure, indicated by the diffuse intensity and offset of the peak position from crystalline ω positions in the electron diffraction pattern [50]. Despite several attempts at modeling the incommensurate ω structure, the underlying mechanism is still inconclusive. Our predicted LITs provide insight into this phenomenon, i.e., a high local Nb content will induce LITs, which can enlarge the volume locally and explain the shifted ω peaks in Zr-Nb alloys. Another example is the stabilization of the ω phase in radiation damaged Zr-Nb alloys [51]. Previous experimental studies attribute this to the enhanced density of point defects and suggest that interstitials may play an essential role in stabilizing ω [52,53]. The LITs can be regarded as a set of interstitial chains. Nevertheless, it is still challenging to observe the atomic structure of LITs experimentally, especially other impurities may obscure LITs. The emergence of high-resolution temporal and spatial probes (e.g. Cs-corrected TEM and x-ray diffraction measurements) provide an excellent near-term opportunity to validate our predictions.

ACKNOWLEDGMENTS

This work was supported by the National Natural Science Foundation of China (52171011 and 51931004) and the 111 project 2.0 (BP2018008).

References

[1] K. Otsuka and T. Kakeshita, MRS Bull. **27**, 91 (2002).

[2] D. A. Porter, K. E. Easterling, and M. Y. Sherif, *Phase Transformations in Metals and Alloys* (CRC Press, Boca Raton, FL, 2008).

[3] E. L. Pang, G. B. Olson and C. A. Schuh, Nature **610**, 491 (2022).

[4] Zh. P. Li, T. Mori, F. Ye, D. R. Ou, J. Zou, and J. Drennan, Phys. Rev. B **84**, 180201(R) (2011).

[5] E. Ma, M. Atzmon, Mater. Chem. Phys. **39**, 249 (1995).

[6] P. Y. Cao, F. Y. Tian, Y. D. Wang, Comp. Mater. Sci. **171**, 109277 (2020).

[7] S. E. Haghighi, Y. Liu, G. H. Cao, L. C. Zhang, Mater. Design. **97**, 279 (2016).

[8] G. H. Liu, Z. D. Wang, T. L. Fu, Y. Li, H. T. Liu, T. Li, M. Gong, G. D. Wang, J. Alloy. Compd. **650**, 45 (2015).

[9] R. Davis, H. M. Flower, and D. R. F. West, J. Mater. Sci. **14**, 712 (1979).

[10] G. K. Dey, R. Tewari, S. Banerjee, G. Jyoti, S. C. Gupta, K. D. Joshi and S. K. Sikka, Philos. Mag. Lett. **82**, 333 (2002).

[11] A. Kwiatkowski da Silva, D. Ponge, Z. Peng, G. Inden, Y. Lu, A. Breen, B. Gault and D. Raabe, Nat. Commun. **9**, 1137 (2018).

[12] H. Zhang, J. Y. Zhang, J. P. Hou, D. D. Zhang, Y. H. Yue, G. Liu, J. Sun, Acta Mater. **241**, 118411 (2022).

[13] Q. Zhang, W. S. Lai, and B. X. Liu, Phys. Rev. B **63**, 212102 (2001).

[14] J. Liang, Z. R. Liu, K. Rao, J. X. Hu, D. Y. Li, Phys. Lett. A **30**, 127569 (2021).

[15] H. P. Van Landeghem, B. Langelier, B. Gault, D. Panahi, A. Korinek, G. R. Purdy, H.S. Zurob, Acta Mater. **124**, 536 (2017).

[16] H. Jin, I. Elfimov, M. Militzer, J. Appl. Phys., **123**, 085303 (2018).

[17] S. K. Sikka, Y. K. Vohra, R. Chidambaram, Prog. Mater. Sci. **27**, 245 (1982).

[18] D. E. Fontaine, N. E. Paton, J. C. Williams. Acta. Metall. **19**, 1153 (1971).

[19] B. BORIE, S. L. SASS, A. ANDREASSEN. Acta. Cryst. **29**, 594 (1973).

[20] T. Li, D. Kent, G. Sha, L. T. Stephenson, A. V. Ceguerra, S. P. Ringer, M. S. Dargusch, and J. M. Cairney, Acta Mater. **106**, 353 (2016).

[21] A. Jaworski Jr, S. Ankem, J. Mater. Eng. Perform. **14**, 755 (2005).

[22] D. Doraiswamy, S. Ankem, Acta Mater. **51**, 1607 (2003).

[23] G. M. Benites, A. F. Guillermet, J. Alloys. Compd., **302**, 192 (2000).

[24] M. J. Li, X. H. Min, K. Yao, F. Ye, Acta Mater. **164**, 322 (2019).

[25] Y. F. Zheng, D. Banerjee, H. L. Fraser, Scripta Mater. **116**, 131 (2016).

[26] Q. M. Hu, L. Vitos, and R. Yang, Phys. Rev. B **90**, 054109 (2014).

[27] A. R. Kilmametov, Y. Ivanisenko, A. A. Mazilkin, B. B. Straumal, A. S. Gornakova,

O. B. Fabrichnaya, M. J. Kriegel, D. Rafaja, H. Hahna, Acta Mater. **144**, 337 (2018).
[28] M. J. Li, X. H. Min, Sci. Rep. **10**, 8664 (2020).
[29] S. Plimpton, J. Comput. Phys. **117**, 1 (1995).
[30] B. Schölkopf and A. J. Smola, *Learning with Kernels* (MIT Press, Cambridge, 2002).
[31] See Supplemental Material at for details about the description, benchmark and properties of the machine-learning interatomic potential, which includes Refs. [32–38].
[32] A. Zunger, S. H. Wei, L. G. Ferreira, and J. E. Bernard, Phys. Rev. Lett. **65**, 353 (1990).
[33] S. H. Wei, L. G. Ferreira, J. E. Bernard, and A. Zunger, Phys. Rev. B **42**, 9622 (1990).
[34] A. van de Walle, M. Asta, G. Ceder, CALPHAD **26**, 539 (2002).
[35] G. Kresse and J. Furthmuller, Phys. Rev. B **54**, 11169 (1996).
[36] J. P. Perdew, K. Burke, and M. Ernzerhof, Phys. Rev. Lett. **77**, 3865 (1996).
[37] P. E. Blöchl, Phys. Rev. B **50**, 17953 (1994).
[38] T. Hastie, R. Tibshirani, and J. Friedman, *The elements of statistical learning. data mining, inference, and prediction* (Springer, New York, 2009), 2nd ed.
[39] V. Sahni, K. P. Bohnen, M. K. Harbola, Phys. Rev. A **37**, 1895 (1988).
[40] J. P. Perdew, J. A. Chevary, S. H. Vosko, K. A. Jackson, M. R. Pederson, D. J. Singh, C. Fiolhais, Phys. Rev. B **46**, 6671 (1992).
[41] D. Vanderbilt, Phys. Rev. B **41**, 7892 (1990).
[42] P. M. Derlet, D. Nguyen-Manh, S. L. Dudarev, Phys. Rev. B **76**, 054107 (2007).
[43] W. Schille, J. Nucl. Mater. **233**, 964 (1996).
[44] Y. Cao, V. Fatemi, S. A. Fang, K. Watanabe, T. Taniguchi, E. Kaxiras, P. J. Herrero, Nature **556**, 43 (2018).
[45] K. M. Ho, C. L. Fu, B. N. Harmon, Phys. Rev. B **28**, 6687 (1983).
[46] G. Henkelman, B. P. Uberuaga, and H. Jonsson, J. Chem. Phys. **113**, 9901 (2000).
[47] G. Henkelman and H. Jonsson, J. Chem. Phys. **113**, 9978 (2000).
[48] L. Pauling, J. Am. Chem. Soc. **69**, 542 (1947).
[49] S. K. Menon, S. Banerjee, R. Krishnan. Metall. Trans. A **9**, 1213 (1978).
[50] D. T. Keating, S. J. LaPlaca, J. Phys. Chem. Solids. **35**, 879 (1974).
[51] S. Banerjee, P. Mukhopadhyay, *Phase Transformations: Examples from Titanium and Zirconium Alloys* (Elsevier, Oxford, 2007).
[52] D. de Fontaine, Metall. Mater. Trans. A **19**, 169 (1988).
[53] H. Dosch, A. V. Schwerin, and J. Peisl, Phys. Rev. B **34**, 1654 (1986).

Figure Captions

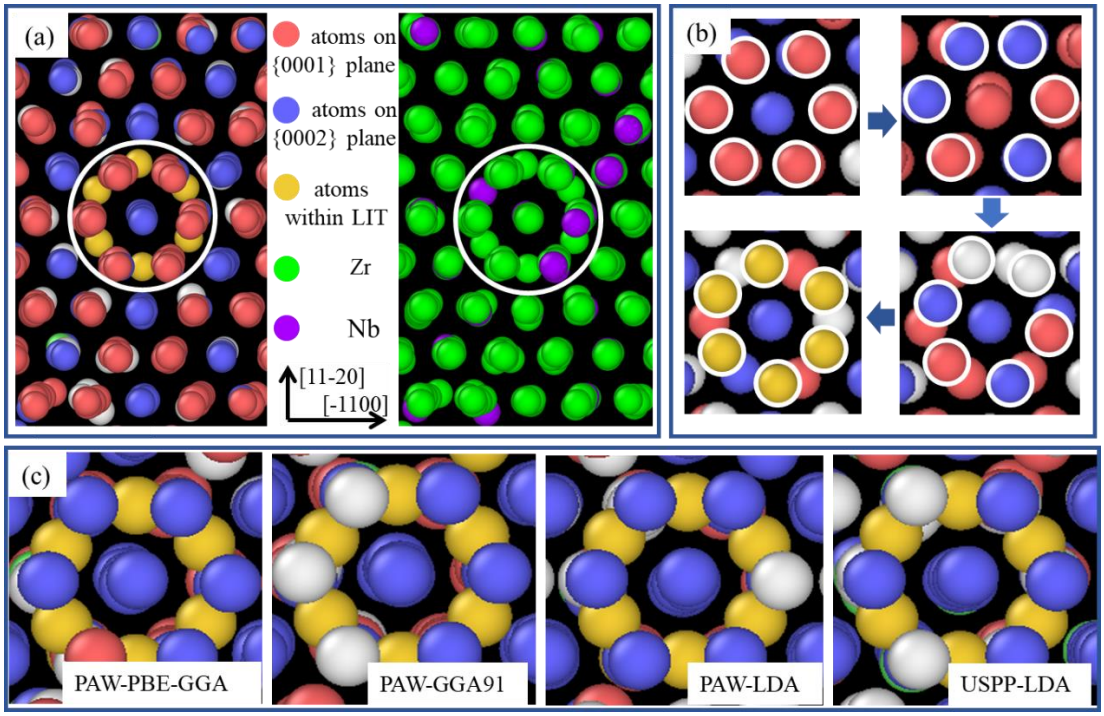

FIG. 1. Molecular dynamic simulation of the Zr-10Nb single crystal showing the formation of LITs. (a) Structure of the Zr-10Nb alloy after ~1 ns MD simulation starting from a perfect ω phase single crystal. Left panel shows the structural information. Blue and red atoms located in {0001} plane and {0002} plane, respectively. Yellow atoms within LIT that marked by white circle. Right panel shows the element distribution in the same atomic configuration. Green atoms present Zr and purple atoms present Nb. (b) The formation process of a local interlayer twist (LIT), where 6 atoms on a {0002} plane co-rotate approximately 30° around the c-axis of the ω phase. (c) Typical microstructure after 6 ps AIMD simulations of the ω phase containing a LIT with different pseudopotentials.

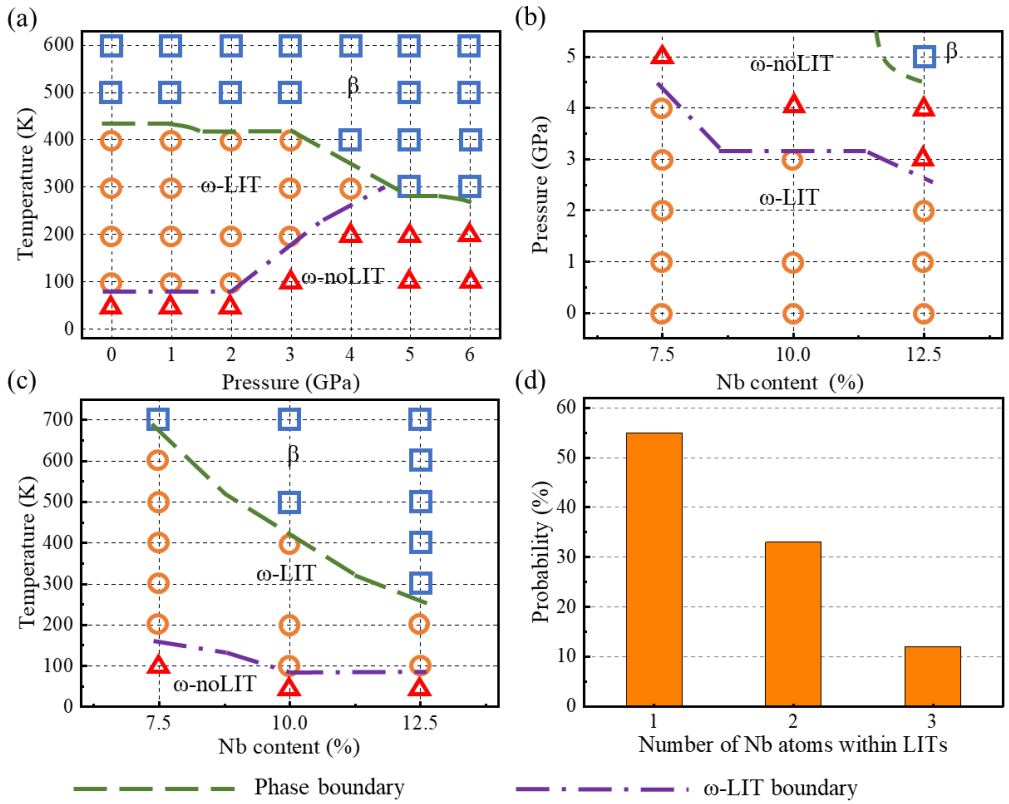

FIG. 2. Phase diagram of Zr-Nb alloys from MD simulations. (a) The temperature–pressure phase diagram showing the stability region of LITs for Zr-10Nb alloys. (b) The stability region of LITs as a function of pressure and Nb content at 200 K. (c) The stability region of LITs as a function of temperature and Nb content at 0 GPa. The cubic, circle and triangle symbols represent the β phase, ω phase with LITs and ω phase without LITs, respectively. The cyan and violet lines show the phase boundaries. (d) Probability distribution of LITs containing different numbers of Nb atoms for Zr-10Nb alloys.

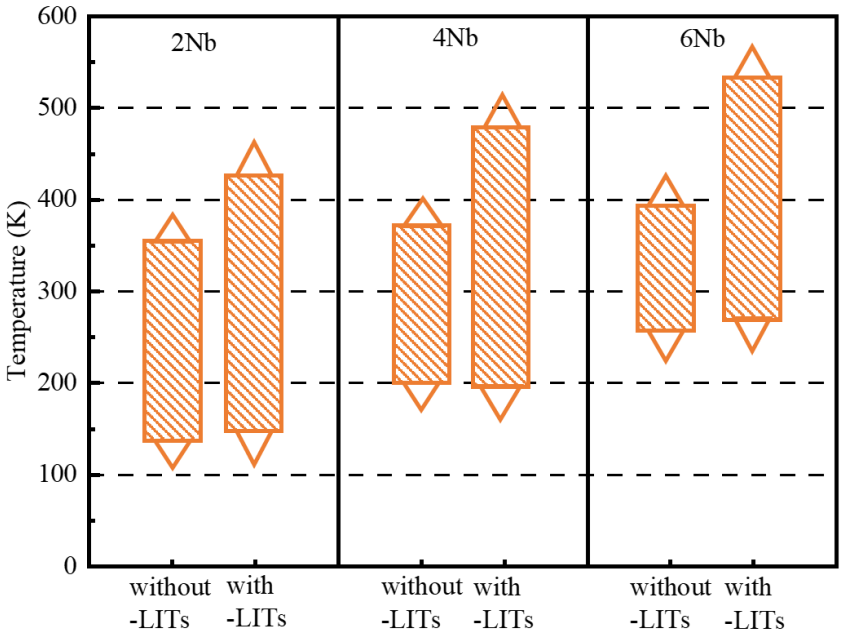

FIG. 3. Comparison of phase transformation temperatures for Zr-10Nb alloys with and without LITs. The three panels show the data of Zr-10Nb samples with different concentration of Nb within LITs, and the chemical arrangements of the systems without LITs are the same. The up-triangle is the transformation temperature upon heating, while the down-triangle represents the transformation upon cooling. The shaded area shows the corresponding thermal hysteresis of the ω↔β phase transformation. X-Nb (X= 2, 4 and 6) represent averaged X Nb atoms within each LIT.

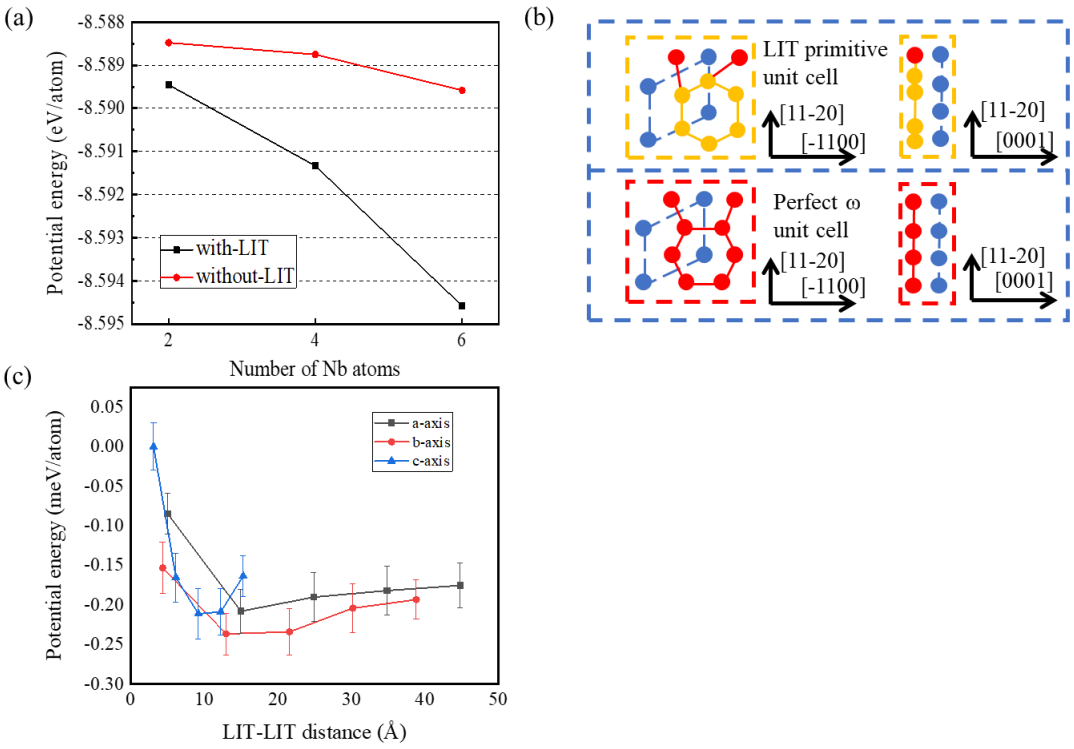

FIG. 4. Thermodynamic stability of ω-phase in Zr-10Nb alloys containing LITs. (a) Potential energy of the Zr-10Nb supercell with and without LITs when different average numbers of Nb atoms are within the LIT and the chemical arrangements of the without LIT systems are the same. (b) Illustration of the primitive unit cell of a LIT (upper panel) and the corresponding perfect ω-phase (lower panel). (c) The change of potential energy for the Zr-10Nb supercell as a function of the LIT-LIT distance along different directions, a-axis is $[11\text{-}20]_{\omega}$, b-axis is $[\text{-}1100]_{\omega}$, c-axis is $[0001]_{\omega}$. The supercell only contains two LITs, and each LIT has 6 Nb atoms. The reference configuration of Zr-10Nb supercell is set as 2 LITs adjacent along c-axis.

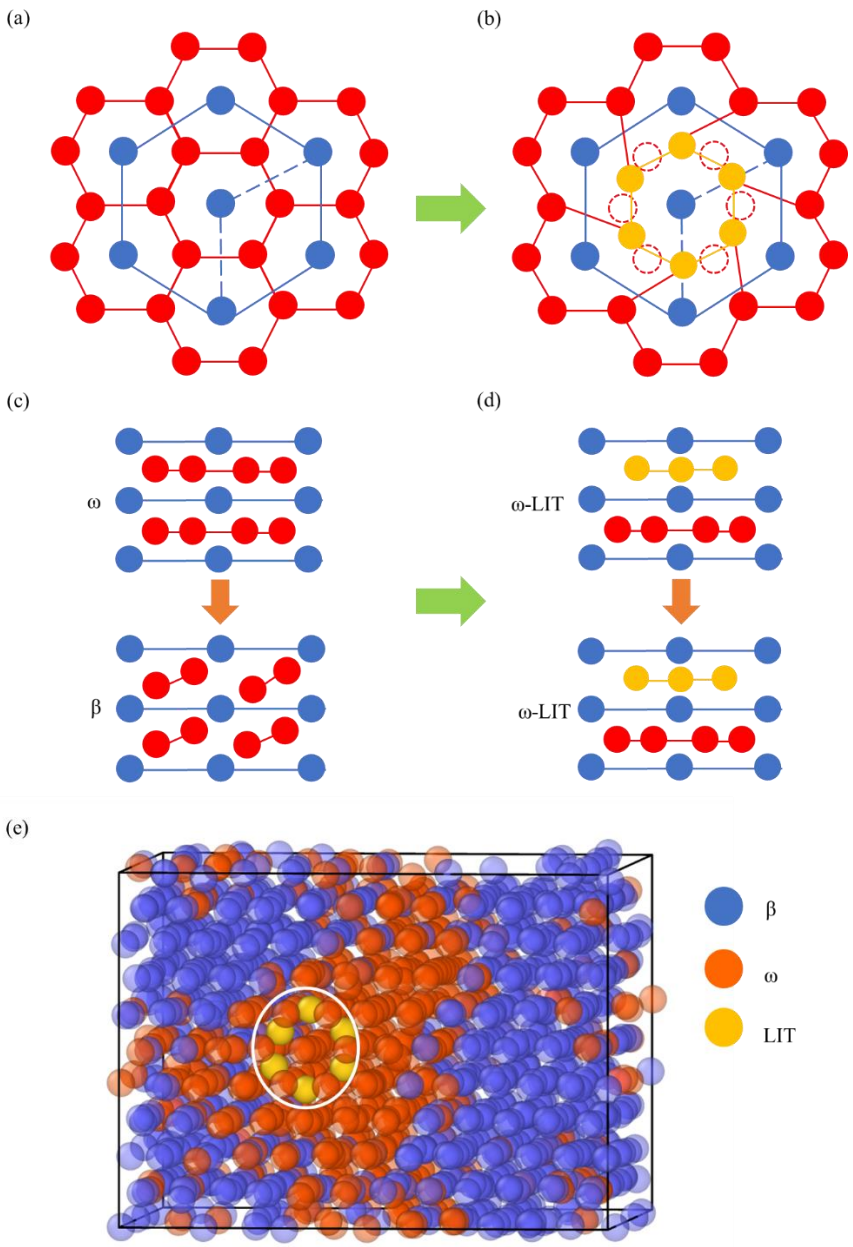

FIG. 5. Effect of LITs on the ω→β phase transformation mechanism. (a, c) Illustration of the $\{0002\}_{\omega}$ decollapse mechanism for the ω→β phase transformation pathway starting from a perfect ω phase. (b, d) Illustration of the ω→β phase transformation pathway inhibited by the LITs. The blue and red atoms are located in the {0001} plane and {0002} plane, respectively. The yellow atoms represent the LIT. (e) MD simulation of Zr-10Nb alloy showing LIT locks ω phase during the heating process. The blue atoms represent the β phase, while the orange atoms are the ω phase, and the yellow atoms belong to the LIT.

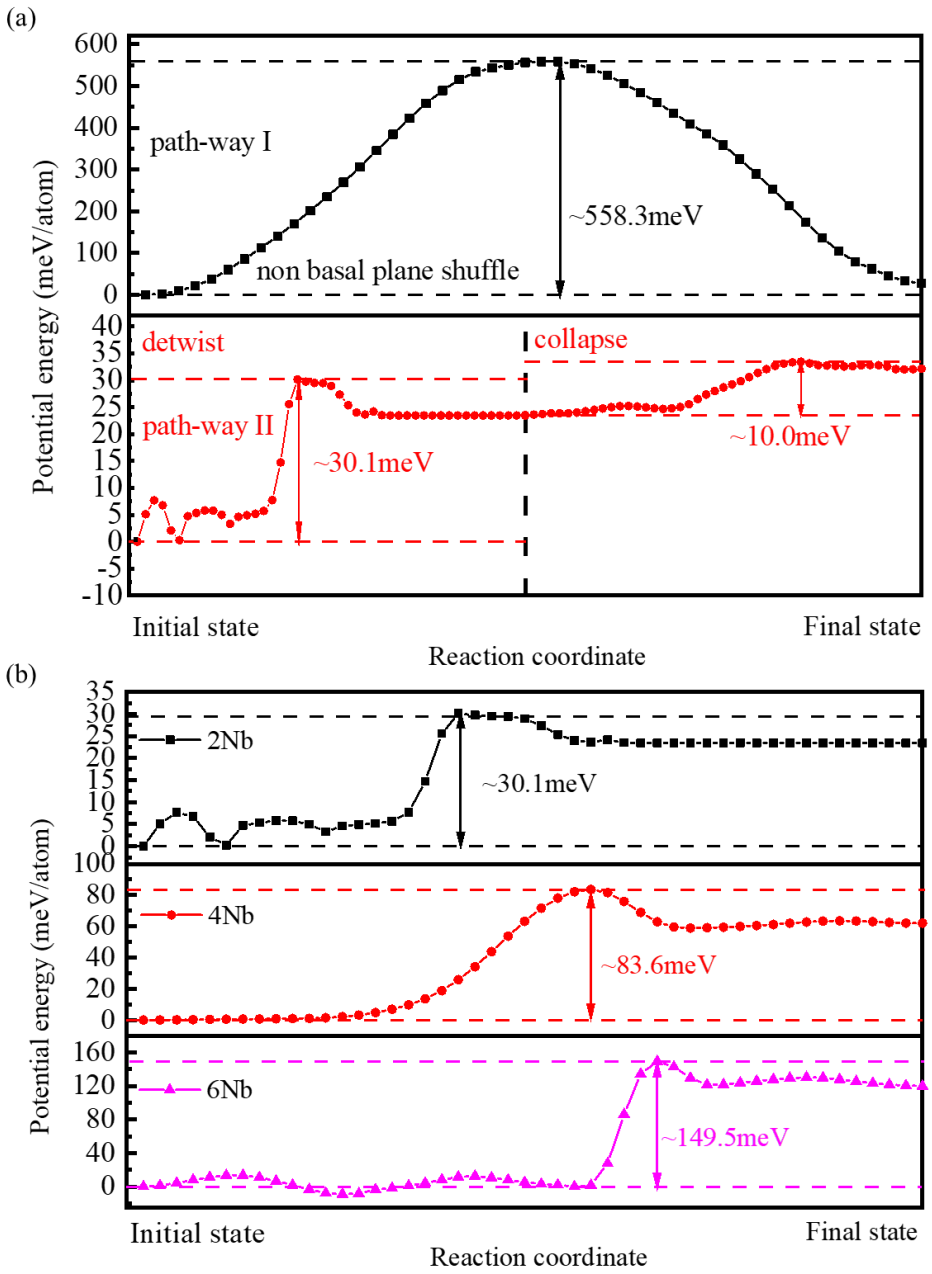

FIG. 6. Potential energy calculated along the ω→β phase transformation pathways by the NEB method. (a) Change in potential energy along the two different transformation pathways. (b) Transformation energy barrier of LITs detwisting for different number of Nb within the LIT.

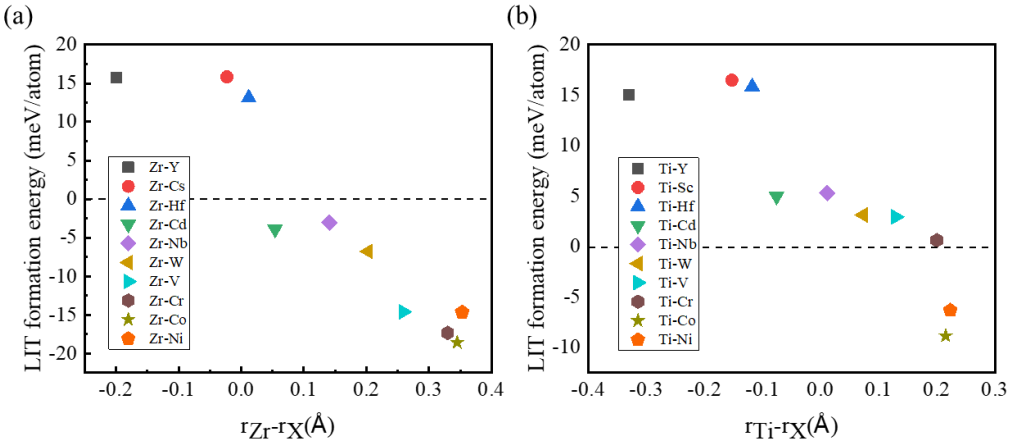

FIG. 7. Formation energy of LITs in different Zr- and Ti-based binary alloys. (a) Formation energy of a LIT in different Zr-X alloys. (b) Formation energy of a LIT in different Ti-X alloys. 6 atoms within the LIT are all solute atoms. The dash line is the threshold of formation energy for stable LITs.

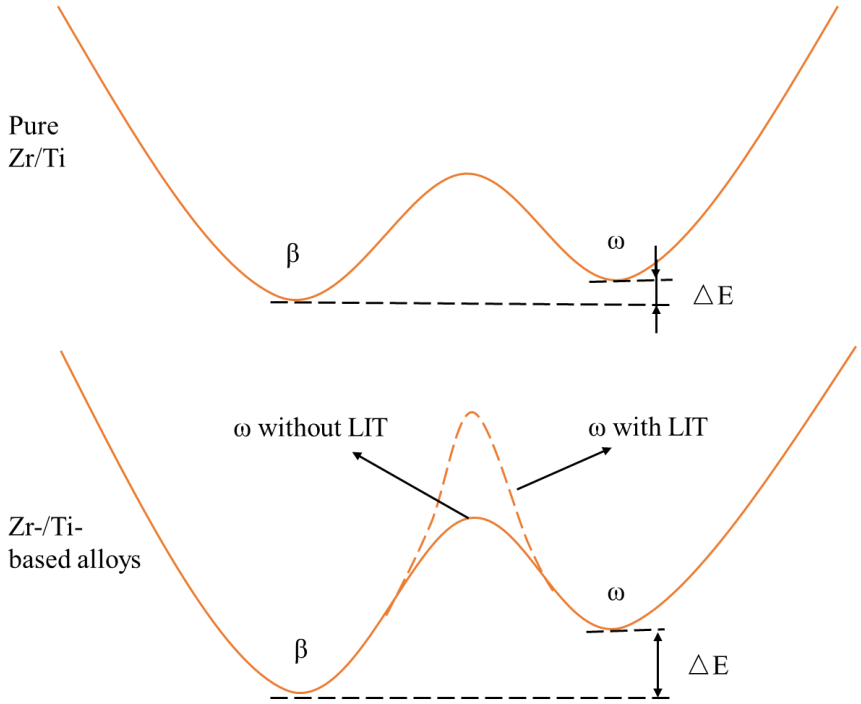

FIG. 8. Illustration of free energy landscape along the β↔ω phase transformation pathway. Dopant atoms decrease the relative free energy of β phase, while the formation of LITs will increase the phase transformation barrier.